ORIGINAL PAPER

Study on the Characteristics of Zinc Oxide Nanocolloid Prepared Using Electrical Spark Discharge Method

Kuo-Hsiung Tseng[1] · Yur-Shan Lin[1] · Hsueh-Chien Ku[1] · Hen-Lin Lee[1]

Abstract

In this study, zinc oxide (ZnO) nanocolloids (ZnONCs) were prepared in an electrical discharge machine using the electrical spark discharge method. ZnONCs comprising ZnO nanoparticles (ZnONPs) and zinc nanoparticles (ZnNPs) could be successfully prepared using metal electrodes with 99.97%-purity zinc (Zn) wire and deionized water as the dielectric fluid at normal temperature and pressure; chemical substances were not required in the preparation. According to the results of ultraviolet–visible spectroscopy, the ZnONP characteristic peak value was 345 nm. X-ray diffraction results indicated that ZnONCs had both Zn and ZnO crystallite orientations. Transmission electron microscopy results revealed that ZnONPs and ZnNPs exhibited elongated crystals measuring 30–50 nm, a ZnO d-spacing of 0.25 nm, and a Zn d-spacing of 0.21 nm. Raman and photoluminescence imaging results indicated favorable structural quality and crystallinity.

Introduction

Zinc is a silvery white transition metal [1] with a density slightly lower than that of iron, with a hexagonal crystal structure [2] and diamagnetic properties [3]. It is a prominent metal often used in, for example, automobile, battery, and construction industries. Zinc oxide, in the form of white powder, is the oxidation product of zinc [4]. The decrease in the size of nano-zinc oxide particles leads to changes in its material properties. Zinc oxide has three crystal structures: wurtzite hexagonal structure, cubic zincblende, and rocksalt, with wurtzite hexagonal structure being the most stable [5]. Due to the hexagonal symmetry of the structure and the lack of a center of symmetry, zinc oxide has excellent piezoelectric properties, which, coupled with its high chemical stability [6] and high effective electromechanical coupling coefficient (8.5%), enables it to be applied to surface acoustic wave devices and film bulk

acoustic wave resonators. Zinc oxide is a group II–VI wide-bandgap semiconductor (3.37 eV) and is a direct bandgap semiconductor at room temperature. It has a large exciton binding energy (60 meV), making it a common material in short-wavelength optoelectronic components such as light-emitting diodes and laser diodes [7]. Because zinc oxide absorbs ultraviolet light but not visible light, does not irritate the skin, and is nontoxic, it is often used in sunscreen. In addition, zinc oxide is listed as generally recognized as safe (GRAS) by the United States Federal Drug Administration; thus, it is also widely applied in biology, medicine, antibacterial, and consumer goods [8–11]. Moreover, novel zinc oxide photocatalyst technology can be used to remove pollutants and reduce the high cost of wastewater treatment [12, 13]. In brief, nano-zinc oxide is a multifunctional metal oxide material.

Common preparation methods include physical vapor deposition [14], hydrothermal synthesis [15], chemical vapor deposition [16], and the sol–gel process [17]. However, ZnO synthesized using solid-phase synthesis [18] contains impurities. Preparation of ZnO using liquid-phase synthesis (e.g., the sol–gel method [19]) involves the use of $Zn(CH_3COO)_2 \cdot 2H_2O$ as the precursor, ethanol as the

✉ Kuo-Hsiung Tseng
khtseng@ee.ntut.edu.tw

1 Department of Electrical Engineering, National Taipei University of Technology, Taipei 10608, Taiwan, ROC

solvent, and NaOH and distilled water as the media. Additionally, preparation using the liquid synthesis requires considerable equipment. Regarding the synthesis of ZnO using the plasma-in-liquid process [20], the Zn electrodes used in the process need to be subjected to complex processing. Furthermore, a low-pressure preparation environment (20 kPa) and coating with Teflon are required for plasma-in-liquid synthesis of ZnO. Currently, the preparation of nano-ZnO is costly. Therefore, costs must be reduced and production efficiency must be increased.

Therefore, this study proposed a new method for preparing nano-ZnO, namely the electrical spark discharge method (ESDM) [21]. In the ESDM preparation process, only an instrument (electrical discharge machine, EDM) and two materials (commercially available Zn wire and deionized water) are required to obtain pure ZnONCs. The preparation method involves subjecting the Zn wire to an electric spark discharge process for 20 min under appropriate EDM control parameters (T_{on}:T_{off}, IP, and HV). The entire process is fast and simple, in that (1) it can be completed in an environment with normal temperature and pressure; (2) the electrode (Zn wire) used does not need to undergo complicated preprocessing; and (3) no precursor, solvent, or medium is required. Because no chemical agents are added, the sample obtained is pure nano-ZnONCs without any derivatives; thus, environmental pollution is avoided. ESDM is a simple, fast, and green preparation method.

Experimental Principle and Method

Experimental Principle

In this study, an electrical discharge machine (EDM) was used to prepare metal nanocolloids. In this method, the upper and lower electrodes were first immersed in the dielectric fluid (either DW or another low-conductivity solution), and a periodic, fast-changing voltage pulse was subsequently applied to the upper and lower electrodes. The voltage pulse generated high energy and temperatures, causing the metal surface of the electrodes to melt and be removed [22]. The EDM parameter configurations included T_{on}:T_{off}, IP, and an HV. T_{on}:T_{off} affects precision during electrical discharge, and it was set in the range of 0–999 μs. IP was set in the range of 1–7 ranks; higher ranks enable larger currents between the electrodes, which accelerate the fabrication process but at a major cost to precision. HV settings toggle between two types of no-load voltages (140 and 240 V). If the metal electrode has a lower discharge as a result of its high melting point or hardness, the machine should be set to 240 V. The EDM

primarily employed electric arc discharge to prepare metal nanoparticles (Fig. 1). In the first phase (a), the discharge-on phase, two electrodes were immersed in low-conductivity dielectric fluid. When electrified, the upper electrode approached the lower electrode, and when they were approximately 30 μm apart [23], the electric field intensity exceeded the withstand voltage of the dielectric fluid, and numerous electrons were injected from the lower electrode to the upper one to form an electric arc. In the second phase (b), the ionization phase, after the insulation between the two electrodes was damaged, the collisions between the ejected electrons and the neutral atoms in the dielectric fluid excited the valence electrons on the atom surface to form cations. At this time, the electrons flowed again toward the upper electrode to form an ionization channel. I_{gap} denotes the rising current formed. In the third phase (c), the melting phase, the ions generated during ionization continued to collide with the upper and lower electrodes, and kinetic energy was converted into thermal energy, which melted the surface metal of the electrodes into nanoparticles. In the fourth phase (d), the discharge-off phase, the power supply was cut, and both V_{gap} and I_{gap} were reduced to 0; the electrodes stopped discharging electrons, and the ionization channel vanished, leaving the nanoparticles to be suspended in the dielectric fluid. In the fifth phase (e), the resumption of insulation, as the electrodes' metal surfaces cooled, the dielectric fluid between the electrodes regained its insulative properties, and the electrical discharge process was completed. After T_{off}, the next iteration had T_{on} beginning at phase one (a).

Experimental Method

In this study, a Zn wire of 99.97% purity and 1-mm diameter was used as the metallic material for the upper and lower electrodes. The dielectric fluid was low-conductivity (1.8 μS/cm) DW. The EDM's environmental parameters are listed in Table 1. T_{on}:T_{off} was set at 30 μs, a
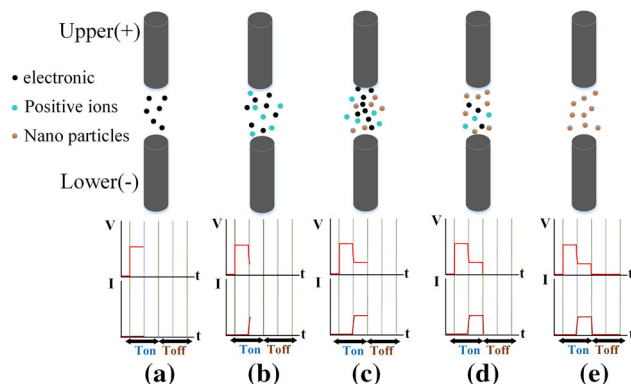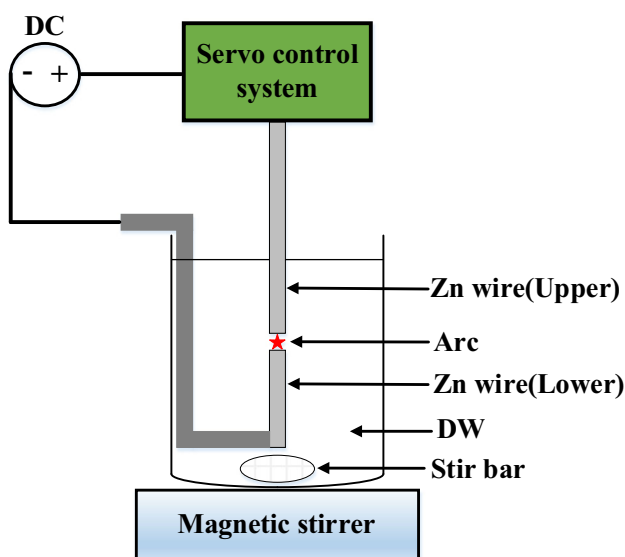

Fig. 1 Schematic of discharge phases: **a** discharge-on, **b** ionization, **c** melting, **d** discharge-off, and **e** resumption of insulation phases

Table 1 EDM environmental parameters in ZnONCs preparation

Pulse cycle	T_{on}:T_{off} = 30:30 (μs)
Material	Zn wire, 99.97%
Diameter of materials	1 mm
Dielectric fluid	DW
Capacity	200 mL
Current segment setting	1
Voltage	140 V
Discharge time	20 min

setting that is suitable for the pulse cycle in ZnONCs preparation. IP was set to 1, which reduced electrode depletion and improved precision. Because the hardness and melting point of the Zn wire were within the EDM's normal discharge range, the HV was set to 140 V. The discharge duration was 20 min. Furthermore, before the discharge was activated, a magnet was placed within the container, and the container was placed on the magnetic stirrer. This ensured that the ZnO nanoparticles (ZnONPs) and Zn nanoparticles (ZnNPs) generated during the discharge process were successfully dispersed in the DW. Once the settings were input, ZnONCs preparation using the EDM was initiated. Figure 2 displays the system schematic.

The ZnONCs preparation was completed after the discharge duration. The optical properties, attributes, and crystal defects were tested using five instruments to verify whether ZnONP and ZnNP were indeed yielded. To determine whether the product had the optical properties of ZnONP, ultraviolet–visible (UV–Vis) spectroscopy was used to obtain data regarding wavelengths and absorption

peak values [24]. X-ray diffraction (XRD) was used to determine the crystalline structure, orientation, and diffraction peak in the analysis of ZnONCs composition [25]. Transmission electron microscopy (TEM) was used to determine the microscopic grain size, distribution, and crystal lattice gaps [26]; crystal orientation was also determined through d-spacing results obtained in accordance with the Joint Committee on Powder Diffraction Standards (JCPDS). Raman testing was used to determine the chemical structure, lattice vibrational pattern, and presence of defects [27]. Photoluminescence (PL) testing was used to determine optical properties as well as the relationship between luminous intensity and crystallization [28].

Results and Discussion

UV–Vis Results

The UV–Vis spectroscopy results are displayed in Fig. 3. According to these results, light absorption decreased as the light wavelength increased. These match those of typical ZnONP spectrograms, where the absorption rate and wavelength are negatively related and the ZnONP characteristic peak value is in the region of 345 nm.

XRD Patterns

The XRD results (Fig. 4) indicated that ZnONCs had crystalline orientations of both ZnO (JCPDS 01-079-0205) and Zn (JCPDS 96-901-2436). The ZnO Bragg angles were 31°, 34°, 36°, 47°, 56°, 63°, 66°, and 68°, and the crystallographic planes, in order, were (100), (002), (101), (102), (110), (103), (112), and (201). The Zn Bragg angles were 36°, 39°, 43°, 54°, 70°, and 70.7°, and the

Fig. 2 System schematic of the EDM
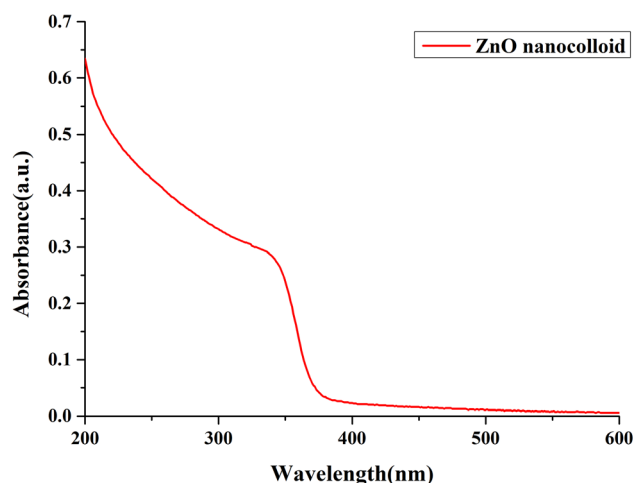
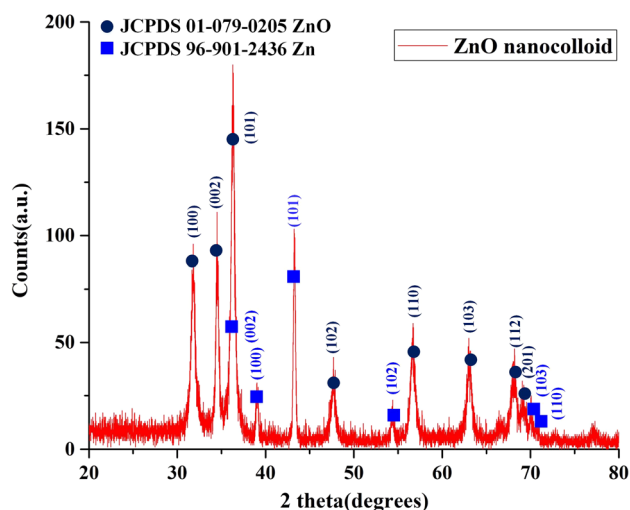**Fig. 3** UV–Vis spectroscopy results for ZnONCs

Fig. 4 XRD patterns of ZnONCs

crystallographic planes, in order, were (002), (100), (101), (102), (103), and (110). The diffraction rays for three of the angles (31°, 34°, and 36°) were ZnO diffraction peaks, indicating that the ESDM-prepared ZnONCs contained no other derivatives except ZnO and Zn crystal structures.

TEM Results

The crystal structure of ZnO is hexagonal wurtzite. After pure zinc was prepared into ZnONCs using the EDM, the crystals' size, shape, and distribution were observed through TEM. The results indicated that both ZnONP and ZnNP groups existed independently in the ZnONCs sample. In the results illustrated in Fig. 5a, the ZnONCs, prepared using spark discharge, exhibited concentrated distributions of elongated crystals. The ZnONP length was approximately 30–50 nm, and its width was approximately 10–20 nm. Figure 5b depicts an enhanced version of the image in Fig. 5a, in which distinct lattice lines of different orientations can be seen. The spacing between the lattice lines (d-spacing) was 0.25 mm; this spacing was attributed to the XRD crystallographic plane (101), which is a classic ZnONP representational result. Figure 5c depicts a ZnONCs image captured from another angle, indicating the presence of elongated crystals and concentrated distributions. Figure 5d presents an enhanced version of the image in Fig. 5c, displaying neat lattice lines with a d-spacing of 0.21 nm. The XRD (JCPDS 96-901-2436) results demonstrated that the nanoparticles were elongated ZnNPs.

Raman and PL Results

The ZnONCs Raman spectrogram is displayed in Fig. 6a. A peak E2(H) corresponding to scattering vibrations was observed at 412 cm^{-1}. This peak is characteristic of ZnO
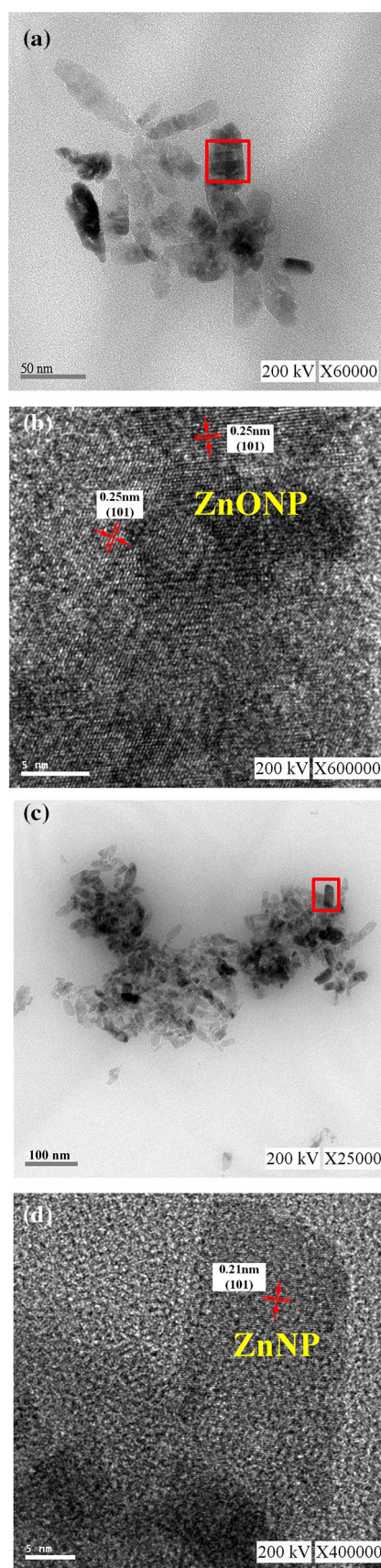
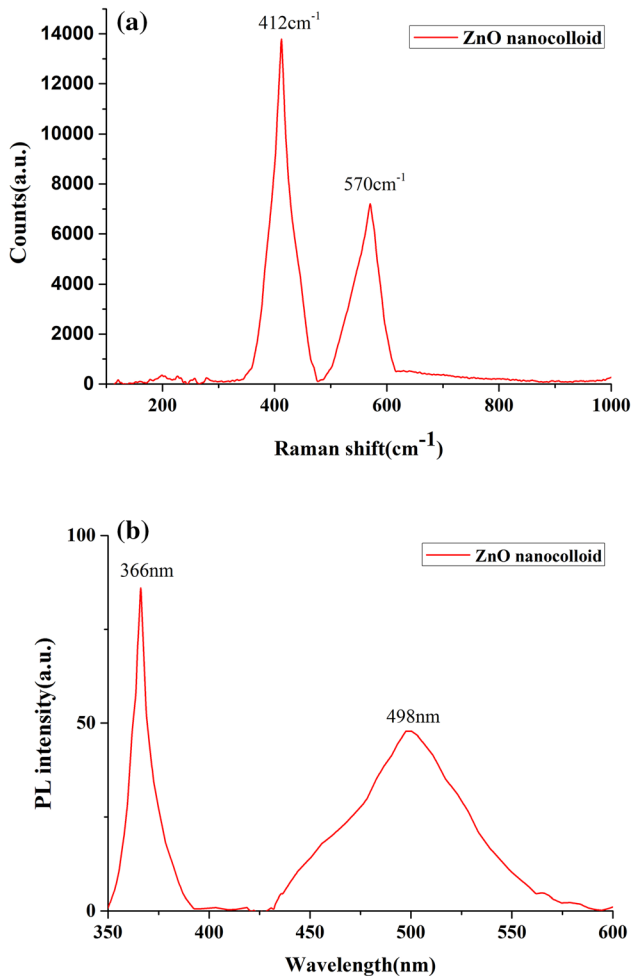◄Fig. 5 TEM images of **a**, **b** ZnONP and **c**, **d** ZnNP

Fig. 6 Spectra of ZnONCs **a** Raman, and **b** PL

crystals and is unrelated to ZnO size. At 570 cm^{-1}, the scattering peak E1(LO) vibrations were caused by oxygen vacancy, zinc interstitials, and their compound. This sample generated only two Raman characteristic peaks, namely E1(LO) and E2(H); no other Raman peaks were formed. The Raman scattering analysis demonstrated the high quality of the ZnO structure in addition to an absence of electric field effects and an unfavorable crystal orientation. The ZnONCs PL spectrum in Fig. 6 exhibits two fluorescence peaks: the thinner peak, namely a UV fluorescence peak (366 nm), and the wider peak, namely a green fluorescence peak (498 nm). UV fluorescence is a near-band-edge emission and is related to the material's intrinsic nature; high luminosity demonstrates strong crystallization. The green fluorescence peak at 498 nm was caused by ZnO nanodefects and was a deep-level emission; its luminosity

was weaker, demonstrating the relatively strong crystallization of the yielded ZnONCs.

Conclusions

In this study, ZnONCs comprising ZnONPs and ZnNPs were successfully prepared in an NTP environment in the first-ever use of the ESDM through an EDM. The contributions of this study are as follows.

1. The ESDM resulted in the successful preparation of ZnONCs. This method is fast, simple, and environmentally friendly because it requires no additional chemical agents in the preparation process.
2. The ZnONCs optical properties were clearly determined through UV–Vis spectroscopy and PL imaging. According to the UV–Vis results, the characteristic peak observed for ZnONP was at 345 nm, indicating high light absorption. According to the PL results, the peak value at 366 nm was higher than that at 498 nm, signifying strong crystallizations in the ZnONCs.
3. Both ZnONPs and ZnNPs existed independently in the derived ZnONCs. This was indicated in a comparison of the d-spacing measurements against the XRD results using (microscopic-scale) TEM imaging of the ZnONCs.
4. High structural quality was indicated by the two classic ZnONCs characteristic peaks in the Raman results.

Compliance with Ethical Standards

References

1. F. Albarède (2004). *Rev. Mineral. Geochem.* **55**, 409–427.
2. Y. Peng, A. W. Xu, B. Deng, M. Antonietti, and H. Cölfen (2006). *J. Phys. Chem. B* **110**, 2988–2993.
3. A. Ogunsipe, J. Y. Chen, and T. Nyokong (2004). *New J. Chem.* **28**, 822–827.
4. Z. L. Wang (2004). *Mater. Today* **7**, 26–33.
5. L. Guo, Y. L. Ji, H. Xu, P. Simon, and Z. Wu (2002). *J. Am. Chem. Soc.* **124**, 14864–14865.
6. C. J. Lee, T. J. Lee, S. C. Lyu, Y. Zhang, H. Ruh, and H. J. Lee (2002). *Applied Physics Letters* **81**, 3648–3650.

7. A. Umar, M. M. Rahman, S. H. Kim, and Y. B. Hahn (2008). *Chem. Commun.* **28**, 166–168.

8. H. Mirzaei and M. Darroudi (2017). *Ceram. Int.* **43**, 907–914.

9. J. P. Shabaaz-Begum (2020). *Stud Indian Place Names* **40**, 186–202.

10. A. Jalali, M. R. Vaezi, N. Naderi, F. T. Abadi, and A. Eftekhari (2020). *Chem Pap* **74**, 253–260.

11. H. Agarwal, S. V. Kumar, and S. Rajeshkumar (2017). *Resource-Eff. Technol* **3**, 406–413.

12. D. Li and H. Haneda (2003). *Chemosphere* **51**, 129–137.

13. D. Rajamanickam and M. Shanthi (2016). *Arab. J. Chem.* **9**, S1858–S1868.

14. G. Jimenez-Cadena, E. Comini, M. Ferroni, A. Vomiero, and G. Sberveglieri (2010). *Mater. Chem. Phys.* **124**, 694–698.

15. B. Liu and H. C. Zeng (2003). *J. Am. Chem. Soc.* **125**, 4430–4431.

16. B. Xiang, P. Wang, X. Zhang, S. A. Dayeh, D. P. Aplin, C. Soci, and D. Wang (2007). *Nano Lett.* **7**, 323–328.

17. H. Li, J. Wang, H. Liu, H. Zhang, and X. Li (2005). *J. Cryst. Growth* **275**, e943–e946.

18. C. A. Angelopoulos, M. Dimitropoulos, A. Govatsi, L. Sygellou, C. D. Tsakiroglou, and S. N. Yannopoulos (2017). *Appl. Catal. B* **205**, 292–301.

19. J. N. Hasnidawani, H. N. Azlina, H. Norita, N. N. Bonnia, S. Ratim, and E. S. Ali (2016). *Procedia Chem.* **19**, 211–216.

20. Y. Hattori, S. Mukasa, H. Toyota, T. Inoue, and S. Nomura (2011). *Mater. Lett.* **65**, 188–190.

21. K. H. Tseng, Y. H. Lin, D. C. Tien, H. C. Ku, and L. Stobinski (2018). *Micro & Nano Letter.* **13**, 1545–1549.

22. K. H. Tseng, C. Y. Chang, M. Y. Chung, and T. S. Cheng (2017). *Nanotechnology* **28**, 465701.

23. K. H. Tseng, J. L. Chiu, H. L. Lee, C. Y. Liao, H. S. Lin, and Y. S. Kao (2015). *Adv. Mater. Sci. Eng.* **8**, 1901334.

24. X. Zeng, J. Yang, L. Shi, L. Li, and M. Gao (2014). *Nanoscale Res. Lett.* **9**, 468.

25. I. Latif, E. E. Al-Abodi, D. H. Badri, and J. Al-Khafagi (2012). *Am. J. Polym. Sci* **2**, 135–140.

26. G. Xiong, H. Luo, J. Zhang, J. Jin, and Y. Wan (2014). *Acta Metall. Sin. (English Letters)* **27**, 656–662.

27. D. N. Montenegro, V. Hortelano, O. Martínez, M. C. Martínez-Tomas, V. Sallet, V. Muñoz-Sanjosé, and J. Jiménez (2013). *J. Phys. D* **46**, 235302.

28. G. Jiangfeng, D. Zhaoming, D. Qingping, X. Yuan, and Z. Weihua (2010). *J. Nanomater.*. https://doi.org/10.1155/2010/740628.